QUARTERLY REPORT

Date of Report: *March 29, 2005*

Contract Number: *DTRS56-04-T-0002>*

Prepared for: *DOT, PRCI, SoCal Gas, Gaz de France, and Valero Energy*

Project Title: *Determining Integrity Reassessment Intervals Through Corrosion Rate Modeling and Monitoring*

Prepared by: *Southwest Research Institute*

For quarterly period ending: *March 31, 2005*

Table 1. Activities and Milestone Status Summary

Activity #	Task #	Activity/Milestone	Expected Date	Status
6	3.2	Set up experiments for external corrosion validation	3/31/2005	Experimental design complete. Set up being initiated
7	2.1	Identify factors that could affect corrosion rates for gas and liquid lines	3/31/2005	Preliminary identification complete
8	2.1	Modify reaction rate parameters and boundary conditions for internal corrosion and debug	4/30/2005	Initial calculations performed
9	1.3	Perform calculations of different scenarios and derive corrosion rates	5/31/2005	Calculations performed for some cases

TECHNICAL STATUS

Computer Modeling of Disbonded Coating Corrosion Rates/Chemistry

As a first step in modeling corrosion under shielded coating, the case of a conductive soil solution with a coating impermeable to electrolyte was modeled. Two types of common crevice geometries found in the field, rectangular shape usually associated with disdonded high-density polyethylene (HDPE) coating and disc shape with fusion-bonded epoxy (FEB) coating were used in the modeling. The effects of crevice length, levels of CP, resistivity of the solution, permeation of O_2 through the coating, the geometrical parameters of the crevice (gap, holiday size and coating thickness) and environment temperature on the crevice steel potential and corrosion rate were modeled.

Figure 1 shows the model geometry where half the disbonded area is drawn due to symmetry of the crevice. The geometry has two domains connected via the holiday mouth. The upper domain, curved square, represents soil chemistry. Its top and right boundaries are assumed to be where a reference electrode and an O_2 concentration probe are located to measure the local pipe potential and O_2 concentration there. These artificial boundaries can be varied without increasing complications of the modeling. In Figure 1, the left boundary is a symmetry line. The coordinates used for modeling, z and y, are labeled, as well as the gap between coating and the steel surface (δ_s) and coating thickness (δ_c).

Due to the comparatively small dimension of the crevice holiday to the upper domain and the fact that O_2 does not diffuse far inside of the crevice, it is reasonable to expect that the potential and O_2 concentration have approximately symmetrical distribution around the crevice holiday. Also, since the IR drop in the bulk soil is insignificant due to the large soil volume area through which the imposed current can pass, the potential on the top and right boundary of the upper domain can be assumed uniform. This is especially true when the imposed CP is not so significant to result in a large "current" or a considerable IR. Although there is always a linear decrease of O_2 concentration from the top and right boundaries before reaching close to the holiday, its nature of approximately symmetrical distribution in this geometry should allow for an assumption of uniform distribution along the top and right boundaries of the upper domain. In this work, the potential measured in the domains is all referenced to saturated $Cu/CuSO_4$.

Although this work is expected to improve over previous modeling of crevice corrosion, the Laplace's equation for potential however constrains the ionic chemical composition of the crevice solution to be uniform throughout the crevice. This has been justified in previous work and not repeated here. To be consistent with previous work, it is assumed that the crevice steel surface is covered by a layer of ferrous hydroxide precipitate which determines the solution chemistry adjacent to the steel surface. The pH there can be calculated from the solubility of this precipitate.

The governing equation to conserve mass of dissolved O_2, expressed by O_2 concentration (c_{O2}), is given by:

$$\frac{\partial^2 c_{O_2}}{\partial z^2} + \frac{\partial^2 c_{O_2}}{\partial y^2} = 0 \qquad (1)$$

Charge conservation, expressed by steel potential measured by a reference electrode in any location in the solution (ψ), is given by:

$$\frac{\partial^2 \psi}{\partial z^2} + \frac{\partial^2 \psi}{\partial y^2} = 0 \qquad (2)$$

The above couple of Laplace's equations have been solved previously for simplified crevice geometry by reducing the equations from 2D to 1D.

The boundary conditions for solving Equations (1) and (2) are described below. All boundaries except B2 (bottom) and B5 (top, curved and left) have zero flux. B1 (left) is a symmetrical boundary and the other zero flux boundaries are insulation to either current or mass transfer of O_2. Although this model is not constrained to that, the coating is here assumed impermeable to ions and O_2. As justified earlier B5 is a boundary with uniform potential and uniform O_2 concentration. Here, the anodes buried in soil far from the domains are assumed to offer no effect on the uniformity of the measured potential along the top and right boundaries. B2 is the crevice steel on which anodic and cathodic reactions occur. The anodic reaction is iron oxidation:

$$Fe \rightarrow Fe^{2+} + 2e^{-} \tag{3}$$

In this alkaline solution, neglecting hydrogen ion reduction the cathodic reactions are: water reduction:

$$H_2O + e^{-} \rightarrow H + OH^{-} \tag{4}$$

and O_2 reduction:

$$O_2 + 2H_2O + 4e^{-} \rightarrow 4OH^{-} \tag{5}$$

The kinetics of the anodic and cathodic reactions can be described by the Butler-Volmer equation. Although Tafel equation is sufficiently accurate for water and O_2 reductions, it may become inappropriate for iron oxidation when the steel surface near holiday area is cathodically polarized highly enough to render the iron vs. ferrous redox current density near its exchange current density.

At B2, the flux of O_2 equals the O_2 reduction rate:

$$-D_{O_2}\left.\frac{dc_{O_2}}{dy}\right|_{y=0} = i_{O_2}/n_{O_2}F \tag{6}$$

Following ohm's law, the flux of potential equals the net current density multiplied by solution resistivity (ρ):

$$\left.\frac{d\psi}{dy}\right|_{y=0} = -\rho(i_{corr} + i_{O_2} + i_{H_2O}) \tag{7}$$

Note that ψ has reverse sign to electrostatic potential defined in electrochemistry.

With a reference electrode placed at B5 to measure the pipe potential (ψ_0), the potential anywhere in the solution is: $\psi = \psi_0 - \chi$, where χ is the electrostatic potential in the solution. With uniform ionic composition in solution, the anodic and cathodic reactions at B2 can be written as:

Butler-Volmer equation for iron vs. ferrous ion being:

$$i_{corr} = i^0_{Fe}\left(10^{\frac{\psi_s - E^{eq}_{Fe}}{b_{Fe}}} - 10^{\frac{-\psi_s + E^{eq}_{Fe}}{b_{Fec}}}\right) \tag{8}$$

Tafel equations for water and O_2 reductions being:

$$i_{H_2O} = -i^0_{H_2O}10^{\frac{-\psi_s + E^{eq}_{H_2O}}{b_{H_2O}}} \tag{9}$$

$$i_{O_2} = -i^0_{O_2\,Ref}\frac{c_{O_2 s}}{c_{O_2\,Ref}}10^{\frac{-\psi_s + E^{eq\,Ref}_{O_2}}{b_{O_2}}} \tag{10}$$

where ψ_s is ψ at the steel surface in the crevice.

Note that the exchange current densities and equilibrium potentials of iron vs. ferrous ion redox and water reduction are not dependent on locations on the steel surface due to uniform ionic composition. Their values can be taken at a reference condition where their values are known. Since the equilibrium potential and exchange current density of O_2 reduction each depends on chemistry, they will have to be calculated first from a known chemistry according to their dependence on chemistry. In order to use a known exchange current density and corresponding equilibrium potential at a known reference condition, a concentration ratio term has to be added to i_{O2} as shown in Equation (10). The reference chemistry of 1 atm O_2 pressure and pH 9 are used in this work to calculate c_{O2Ref} and $E_{O_2}^{eqRef}$.

Table 1 shows the geometrical parameters and conditions used to solve for the crevice corrosion. Although the holiday mouth length is 2 mm, only half (1 mm) is shown due to symmetry of the crevice geometry. The crevice gap is 0.5 mm, comparable to disbondment sizes from different types of coatings. Fusion bonded epoxy (FBE) coating is associated with a thinner disbondment than HDPE coating. The crevice length is here chosen to be long enough to simulate HDPE disbondment (200 times of the gap), although this length is not restricted to vary. Boundary B5 is assumed to be about 1 cm away from the holiday, far enough to meet the assumption of uniform O_2 concentration and uniform potential along that boundary, where the potential and concentration should not be affected significantly by reactions in the crevice. Either the potential measured by a CSE placed at B5 is assumed when there is CP or for the case without CP zero potential flux or current through B5 is assumed. The latter boundary condition allows for the calculation of potential at B5. Assumption of O_2 concentration along B5 may be arbitrary because it depends on how aerated the soil is. It is here for being conservative assumed to be 0.21 atm. The soil resistivity in this work is assumed 25 ohm.m. Temperature of 25 ^oC and total pressure of 1 atm is assumed throughout this work.

Table 1: Geometrical Parameters and Modeling Conditions

Holiday length (m)	0.002	Solution resistivity (ohm.m)	25
Crevice gap (m)	0.0005	Temperature (^oC)	25
Crevice length (m)	0.1	Total pressure (atm)	1
Between steel and top (m)	0.01		
Width of upper domain (m)	0.01		

Results and Discussion

Without CP

When soil resistivity is high due to dry soil condition or due to rocks or other non-ionic-conductive materials blocking CP current from passing to the pipeline holiday area, the current flux passing across B5 can be assumed to be zero. With this and other boundary conditions, Equations (1) and (2) are solved for O_2 concentration (all converted to its partial pressure according to Henry's law) and steel potential measured in the entire domains.

Figure 2 is a contour plot of O_2 partial pressure. The dashed line is drawn in the figure to be used later. Between adjacent contour lines an interval of 0.021 atm is used. The axes are labeled as ratios of x and y dimensions to the gap size. O_2 does not diffuse

deep inside the crevice, within a few gap sizes only, because of limitation of O_2 diffusion compared to its reduction kinetics at the steel surface. Since reduction of O_2 occurs only at the steel surface (ferrous ion oxidation is neglected due to its insignificance to O_2 transport in aqueous solution), the contour line density is greatest near steel surface and decreases as the distance increases toward the soil bulk solution. A plot of O_2 pressure along the arbitrary line in the figure starting from the origin to the position (10,20) is shown in Figure 3. The sharper decrease in O_2 pressure near the origin results from consumption of O_2 at the steel surface by the anodic reaction: iron oxidation. Not participating any reaction in solution, the linear diffusion of O_2 rather has a curvature between 5-15 of z/a because of deformation of the geometry when approaching to the holiday. The holiday mouth is not symmetrically placed with the outer boundary B5.

A clearer view of the O_2 pressure contour lines near the steel surface, where dissolved O_2 pressure varies more significantly, is shown in Figure 4a. Due to slow diffusion, the dissolved O_2 pressure has a varying gradient in the holiday solution decreases from the steel surface into solution. Relatively flat contour lines are observed in the direction parallel with the steel surface and across the holiday mouth. Figure 4b shows contour plot of potential near the holiday mouth. Although the potential does not seem to have a uniform distribution near the holiday region due to the very small potential interval used for the contour (0.2 mV), the potential variation near the holiday region is in fact actually trivial. Slightly moving into the crevice, the contour lines are parallel with each other perpendicular to the steel surface, indicating uniform potential in the crevice perpendicular to the steel surface. It may be noted that the potential around the bottom left corner has a potential greater than the potential at the measure boundary (the highest potential located right at the corner is -0.835 V). This is because of O_2 reduction which anodically polarizing the steel surface still overbalances the internal cathodic polarization due to the internal current flow.

Effect of CP

The effect of CP on the crevice potential at the steel surface is shown in Figure 5. There is a difference between potential at the left point of the steel surface and the given potential at Boundary B5 resulting from IR drop. As expected, the more negative the potential at the measure boundary B5 the more negative the crevice potential. With insufficient CP where potential at boundary B5 is more positive than -0.8705 V, O_2 in the crevice is not reduced sufficiently by external CP, the potential decreases into the crevice. At the holiday, O_2 has higher concentration and it results in a higher corrosion rate. The potential becomes more negative inside the crevice as the O_2 concentration diminishes in the solution. At potentials more negative than -0.8705 V at B5, with all O_2 being electrochemically reduced an excess of CP current reduces water. The potential is more negative near the holiday than inside the crevice. This excess CP functions only by promoting hydrogen generation, doing more harm than good to the pipelines under stress. In the alkaline solution, the free corrosion rate is small and should not be a concern. Therefore, for this particular environment, -0.8705 V should considered as a good potential in protection of the pipelines. Since CP exactly reduces O_2 at this potential and this occurs only near the holiday, open circuit potential quickly reaches after only a very short distance near the holiday (CP shielding).

The corresponding corrosion rate in the crevice due to different levels of CP is shown in Figure 6. Similar to the potential in Figure 5, the corrosion rate decreases as CP increases. With insufficient CP, corrosion rate is greatest near the holiday and decreases into the crevice. CP decreases corrosion rate by reducing O_2 near the holiday area. At potential of -0.8705 V, the corrosion rate is nearly uniform inside the crevice where the corrosion rate equals open circuit corrosion rate. Further calculations will be performed considering CO_2 permeation and flow of solution through the crevice.

Internal Corrosion Rate Monitoring

The Multielectrode Array Sensor (MAS) probe was designed as part of a PRCI co-funded study. This was initially tested in the laboratory under high pressures (up to 1500 psi) and in conditions of different $CO_2 + H_2S + O_2$ mixtures and moisture contents. It was shown that the probe was quite responsive to changing conditions and provided corrosion rate information (Figures 7 and 8). The responses of the electrodes covered by abiotic corrosion products and biofilm are compared in Figure 7. It can be seen that the corrosion rate of the biofilm-covered probes is much higher than that of the corrosion-product covered probe. Both electrodes responded at about the same RH (38 to 45 percent). In both cases, there was an initial increase in corrosion rate followed by a slight drop and a more or less constant corrosion after words. When the RH is decreased, the corrosion rate does not drop immediately. This is illustrated in Figure 8. The corrosion rate is plotted as a function of RH as the probe is first subjected to an almost saturated gas mixture and then slowly dried. When the humidity decreases from a high value, the corrosion rate decreases slowly, but does not reach a low corrosion rate until the RH decreases to below about 20%. Note that when the RH is cycled at intermediate values between 40 to 70%, the corrosion rate essentially follows in a reversible manner. During the increasing RH scan (from 20%), the corrosion rate suddenly increases when the RH exceeds 39%. This hysteresis in the corrosion rate between decreasing and increasing RH cycles suggests that the corrosion products retain significant amount of moisture and drying is slow. These results are described in a report submitted to PRCI

After the demonstration of the probe's capabilities in gas streams, the probe was installed in a liquids pipeline o evaluate the corrosion rates in these systems. A figure of the probe, as installed, is shown in Figure 9. The results to date are shown in figure 10. The galvanic probe was installed by the pipeline company prior to the installation of the MAS probe. The trends in corrosion rates between these two probes are the same. However, the MAS probe provides more direct information on the localized corrosion rate.

External Corrosion Validation Experiments

The experimental design is shown schematically in Figure 11. The design is meant to simulate slow flow of the solution through the disbonded region while maintaining aeration and other boundary conditions. Probes at various locations will measure the potential, pH, and corrosion rate distributions as functions of time.

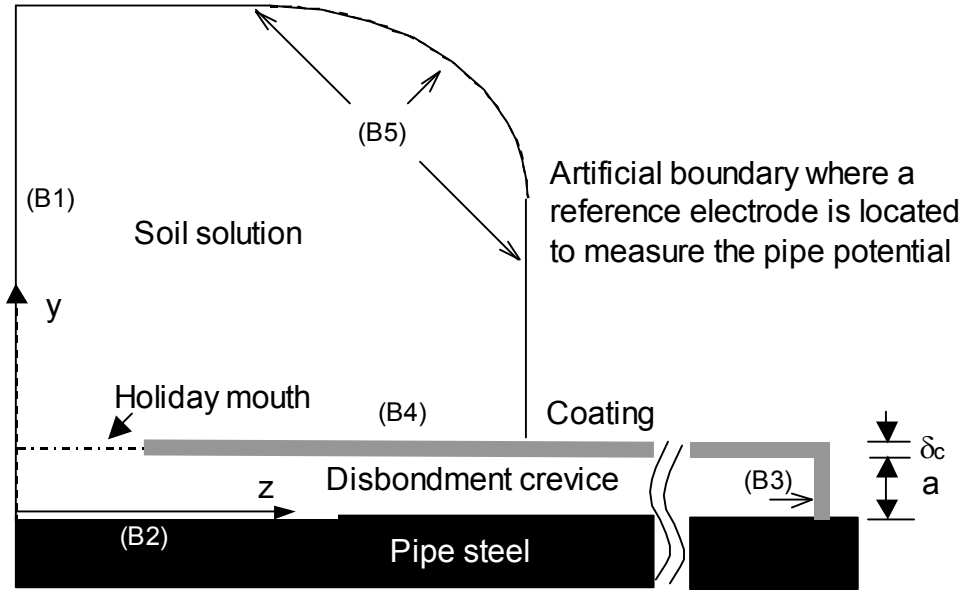

Figure 1: Schematic diagram of the model geometry, with boundaries labeled (B1—symmetry boundary; B2—steel surface, flux boundary; B3 and B4—impermeable coating, no flux boundary; B5—measure boundary, constant O_2 concentration and either zero flux of potential for no CP or constant potential with external polarization).

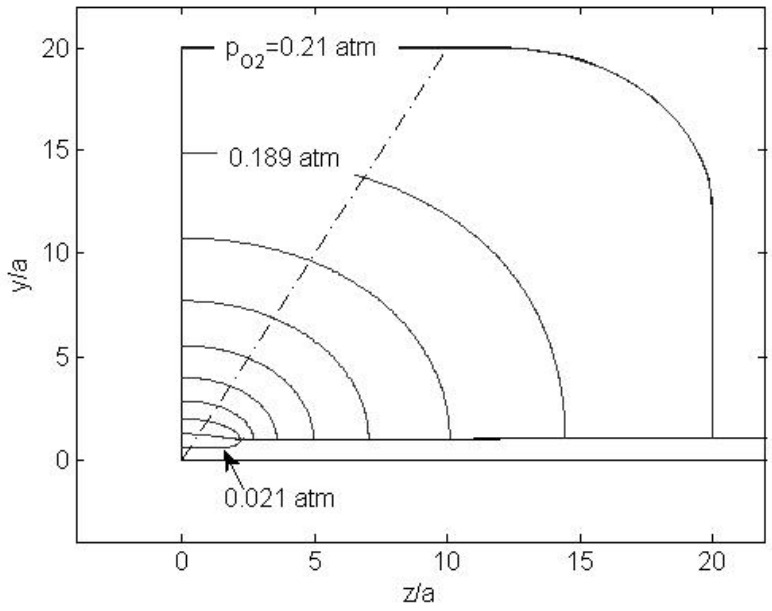

Figure 2: Contour plot of dissolved O_2 partial pressure in and outside of the disbondment crevice.

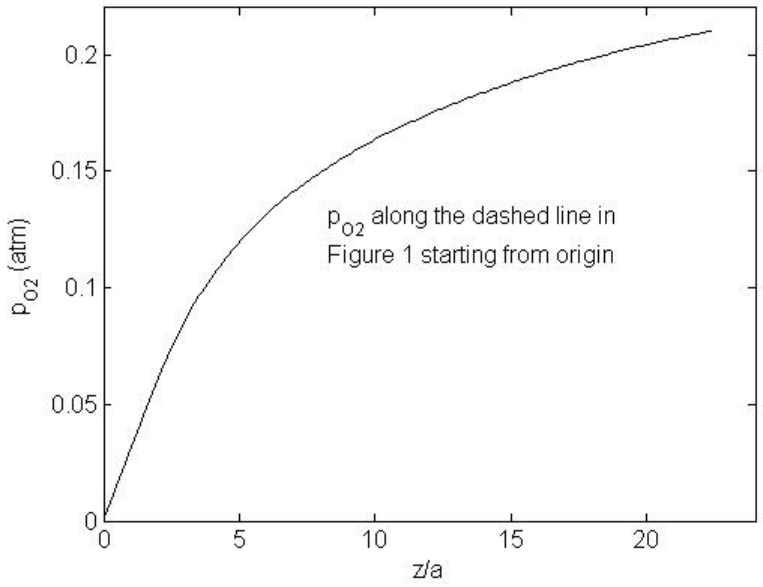

Figure 3: Dissolved O_2 partial pressure along the arbitrary dashed line drawn in Figure 1 starting from the origin.

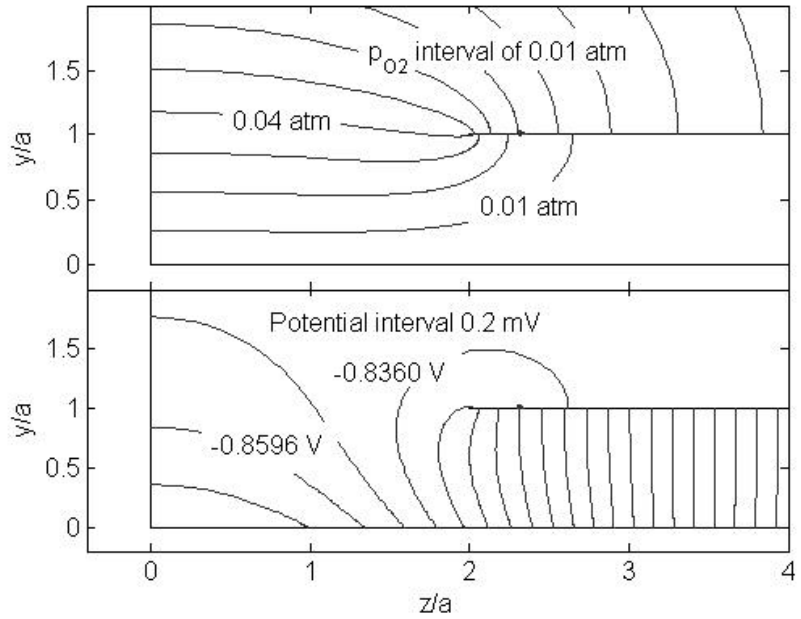

Figure 4: Contour plot of dissolved O_2 partial pressure and crevice steel potential expanded near the holiday.

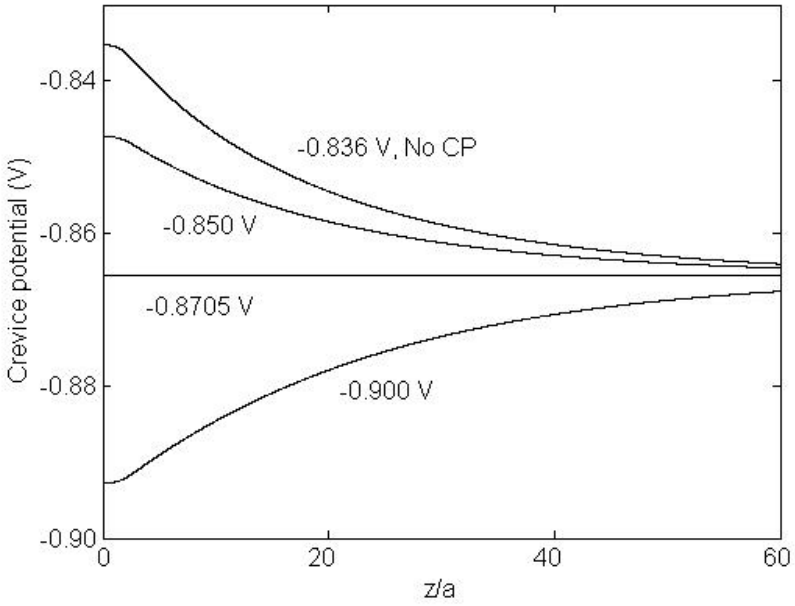

Figure 5: Effect of external CP on crevice potential at the steel surface. Potentials as labeled are steel potentials at the measure boundary B5.

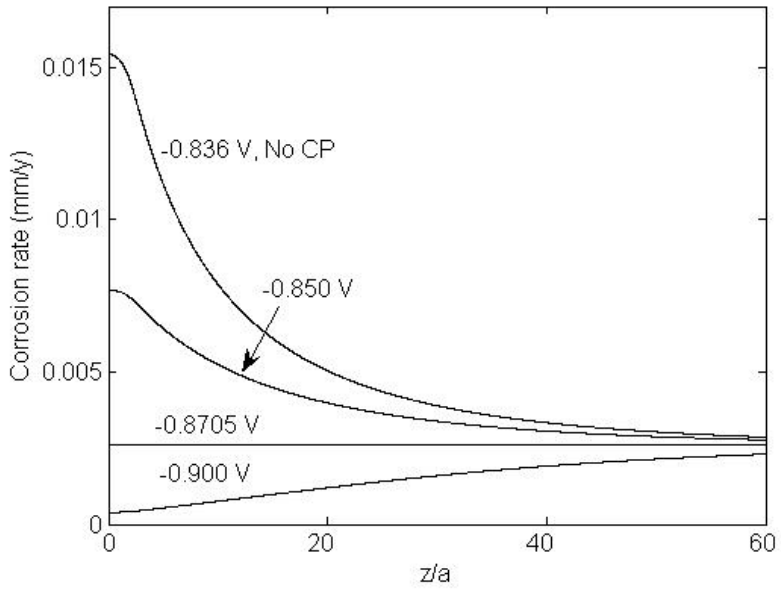

Figure 6: Effect of external CP on crevice steel corrosion rate. Potentials as labeled are steel potentials at the measure boundary B5.

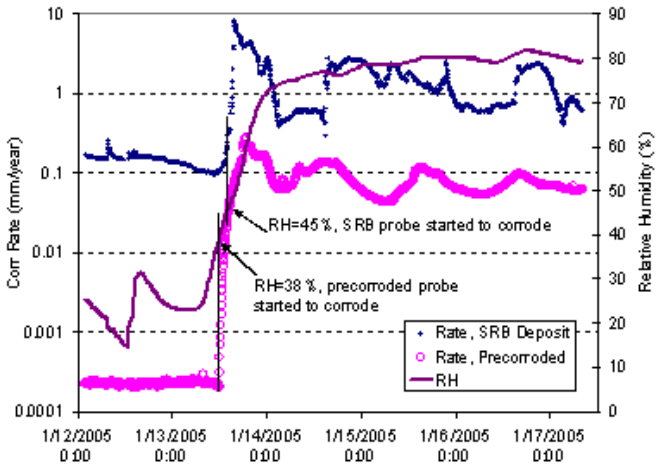

Figure 7. Responses of the localized corrosion rates measured from the probes covered by SRB biofilm and by corrosion products to the increase in relative humidity

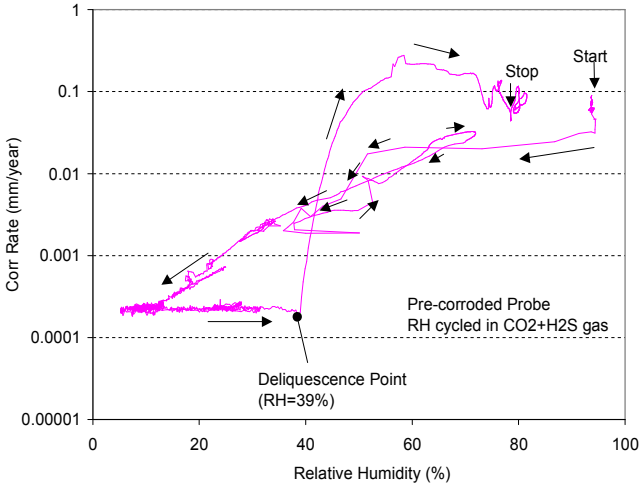

Figure 8. Localized corrosion rate measured from the probes covered by corrosion products as a function of relative humidity. The Arrow in the figures shows the sequence of the test.

Figure 9. MAS probe installed in a liquids line

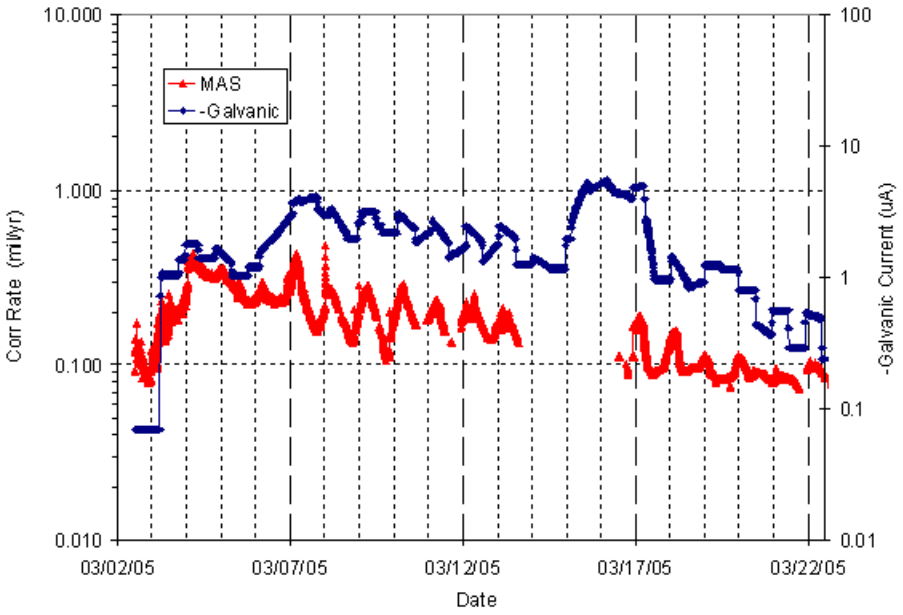

Figure 10. Comparison between the pitting corrosion rate from MAS probe and current signal from Galvanic probe.

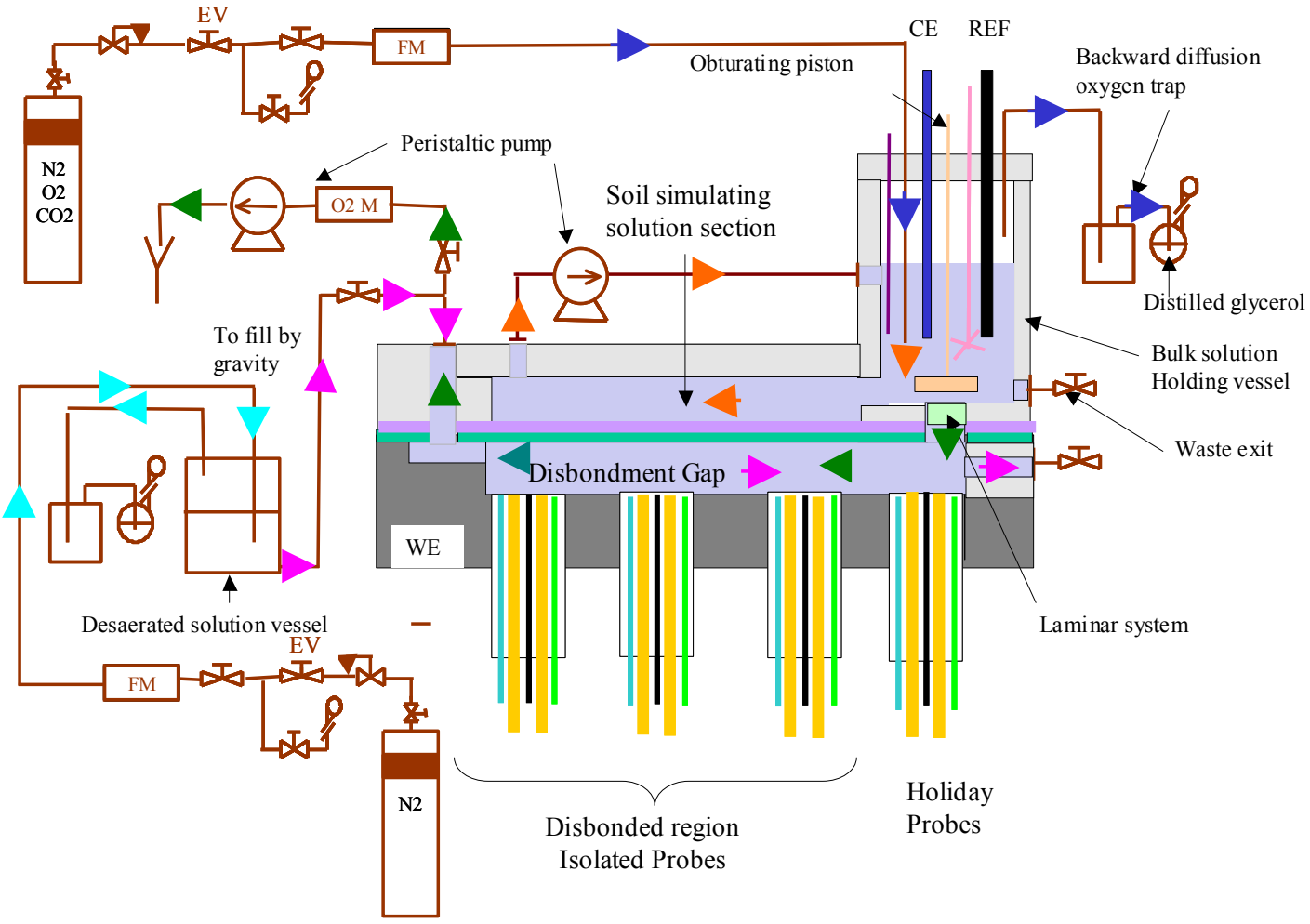

Figure 11. Schematic design of the external corrosion cell for validation of the model

BUSINESS STATUS

- A progress review presentation was made to the Project Manager after the Pipeline R&D forum on March 25, 2005..
- The Gaz de France staff is at SwRI and has started to initiate the external corrosion validation experiments
- The MAS probe has been installed at the Valero plant. Prior to this, the SwRI staff had to take and pass the Coastal Bend Contractors Safety course and the Valero-specific safety course.
- The DOT portion of the funding has been expended slightly over 50 percent. The PRCI cash co-funding has been expended in the development and validation of the MAS probe.

SCHEDULE

Several tasks are in progress and are on schedule.

PAYABLE MILESTONES

Second quarterly report

ISSUES, PROBLEMS OR CHALLENGES

None

PLANNED ACTIVITIES IN THE NEXT 30 TO 60 DAYS

- Continue modeling corrosion rates in disbonded coating using FEMLAB and MATLAB
- Complete data collection from Valero pipeline facilities.
- Obtain data on flow effects from the external corrosion cell
- Hold discussions with other co-funding organizations on field data needs
- Publish a paper on the model results after obtaining the needed permissions.